Available online at www.sciencedirect.com
ScienceDirect
Journal of Crystal Growth 310 (2008) 1847–1852
JOURNAL OF CRYSTAL GROWTH
www.elsevier.com/locate/jcrysgro

Growth of ZnMgO/ZnO films on *r*-plane sapphires by pulsed laser deposition

Mei-Hui Liang[a], Yen-Teng Ho[b], Wei-Lin Wang[a], Chun-Yen Peng[a], Li Chang[a,*]

[a]*Department of Materials Science and Engineering, National Chiao Tung University, 1001, Tahsueh Road, Hsinchu 300, Taiwan*
[b]*Chung-Shan Institute of Science and Technology, Longtan, Taoyuan, Taiwan*

Available online 28 January 2008

Abstract

High-quality ZnMgO/ZnO multi-layer thin films in *a*-plane orientation were grown by pulsed laser deposition on *r*-plane sapphires. Reflection high-energy electron diffraction (RHEED) patterns were performed to monitor the growth morphology and the epitaxy. X-ray diffraction, RHEED, and atomic force microscopy show that anisotropic growth of *a*-plane ZnO results in stripe morphology, and the difference of thermal expansion between ZnO and sapphire plays a significant role on the film surface smoothness. Cross-sectional transmission electron microscopy identifies the cause of disorientation of ZnO growth on sapphire.

PACS: 68.55.Jk; 68.65.Ac; 81.05.Dz

Keywords: A1. Characterization; A3. Laser epitaxy; B1. Oxides; B2. Semiconducting II–VI materials deposition

1. Introduction

As a wide-band-gap semiconductor, ZnO has been recognized as a potential candidate for many devices, such as varistors, light-emitting diodes, laser diodes, transparent conductive films, and photodetectors. Since ZnO possesses a larger exciton binding energy (~59 meV) than other wide-band-gap semiconductors, it is expected that the stability of the exciton offers the possibility to make highly efficient optoelectronic devices.

Emission and absorption of semiconductors can be tuned by means of alloying of different materials and by building quantum wells (QW). Band gap engineering in ZnO can be accomplished using alloys with CdO and MgO. Magnesium incorporation has been shown to increase the band gap of the resulting alloy. The blue shift of the band gap with increasing x for $x \leqslant 0.2$ is approximately linear.

Several studies have already been published on ZnO epilayers and ZnO/(Zn,Mg)O QW prepared by different growth methods. Among various methods for epitaxy of ZnO films, pulsed laser deposition (PLD) is an attractive method as it can deposit a film in a composition close to that of target.

Most of ZnO films grown on *c*-plane or *a*-plane sapphire substrates are in *c*-plane orientation, because *c*-axis orientation perpendicular to the substrates has been found to be a preferable direction of the growth. However, non-polar ZnO is considered to be much more desirable than *c*-plane ZnO in several cases. For example, ZnO has anisotropy along the *c*-axis. Therefore, non-polar ZnO films may be preferable for transverse acting devices such as surface acoustic wave filter. The use of non-polar surfaces is of particular interest since QW structures can be grown without a reduction of the exciton binding energies as demonstrated in non-polar GaN layers [1,2].

The lattice parameter of the wurtzite ZnO structure is $a = 3.2498$ Å, $c = 5.2069$ Å, while the sapphire (Al_2O_3) is rhombohedral ($a = 4.7588$ Å, $c = 12.996$ Å in hexagonal axes). Therefore, the lattice mismatch between ZnO and sapphire along the *c*-axis of ZnO (along [0 0 0 1]) is only 1.53%, whereas the mismatch perpendicular to *c*-axis of ZnO (along [1 0 $\bar{1}$ 0]) is 18.3%. The growth behaviors of ZnO on *r*-plane sapphire can be attributed to the small

*Corresponding author. Tel.: +886 3 5731615; fax: +886 3 5724727.
E-mail address: lichang@cc.nctu.edu.tw (L. Chang).

0022-0248/$ - see front matter © 2007 Elsevier B.V. All rights reserved.
doi:10.1016/j.jcrysgro.2007.11.158

lattice mismatching along the ZnO *c*-axis direction and enhanced lateral growth characteristics. Therefore, the epitaxy relationship between ZnO and *r*-sapphire is known to be $(1\,1\,\bar{2}\,0)_{ZnO}\|(0\,1\,\bar{1}\,2)_{Al_2O_3}$ and $[0\,0\,0\,1]_{ZnO}\|(0\,1\,\bar{1}\,1)_{Al_2O_3}$.

In this work, we have studied the growth of $(1\,1\,\bar{2}\,0)_{Zn_{1-x}Mg_xO}$ ($x=0.2$) and *a*-plane ZnO epilayers grown by PLD on $(0\,1\,\bar{1}\,2)$ sapphire (*r*-plane sapphire). In addition to the growth characteristics [3–9], the growth behavior of $Zn_{0.8}Mg_{0.2}O$/ZnO QW structure grown on *r*-plane sapphire is also reported.

2. Experimental procedure

A KrF excimer laser with $\lambda=248$ nm was used for PLD deposition of ZnO and ZnMgO films. The time duration of the laser pulse was 25 ns, power density was 1–2 J/cm^2, and the pulse frequency was 3 Hz. The base pressure in the growth chamber was 1×10^{-8} Torr. After degreasing in boiled acetone and isopryl alcohol, a 2 in *r*-plane sapphire substrate was loaded into the PLD chamber and heated in high vacuum at 850 °C for 30 min. Then, the oxygen flow was introduced to the chamber in which the oxygen partial pressure was then kept at 1.4×10^{-2} Torr for the rest duration of deposition. The targets in the chamber were 2 in pure ZnO and $Zn_{0.8}Mg_{0.2}O$ sintered ceramics.

For ZnO films, it was deposited in high vacuum for 5 min at 490 °C, and then deposited in oxygen atmosphere at 800 °C for 140 min. As for the ZnMgO/ZnO bilayer growth, ZnO was deposited in vacuum for 2 min at 800 °C, and then deposited in oxygen atmosphere at 800 °C for 22 min, followed by ZnMgO deposition at 650 °C for 59 min. For multi-period ZnMgO/ZnO film structures, the deposition condition for the first ZnO buffer layer was kept the same as described above, followed by the growth of QW at 650 °C with the thickness of each layer varied by changing the deposition time.

The growth process was monitored *in situ* by reflection high-energy electron diffraction (RHEED). The surface morphology was examined by atomic-force microscopy using a DI3100-AFM microscope. High-resolution X-ray diffraction measurements were carried out using a Bede D1 diffractometer in the triple-axis mode. Cu $K\alpha_1$ (1.54056 Å) was selected for incident X-rays by using a Si(2 2 0) monochromator, and no slit was used for the ω scan. Photoluminescence (PL) spectra were acquired using a continuous He–Cd ($\lambda\sim325$ nm) laser as the excitation source. Microstructural characterization was carried out using cross-sectional transmission electron microscopy (TEM) with X-ray energy-dispersive spectroscopy (EDS) for the measurements of chemical compositions.

3. Results and discussion

Fig. 1 shows the XRD pattern of a ZnMgO/ZnO bilayer sample. In addition to the substrate's peaks, only the ZnO *a*-plane $(1\,1\,\bar{2}\,0)$ reflection (~56.5°) appears in $2\theta/\theta$ scan for all the samples. Detailed examination reveals that there are two split peaks at $(1\,1\,\bar{2}\,0)$ reflection which are corresponding to ZnO and $Zn_{0.8}Mg_{0.2}O$, respectively. Using sapphire reflections as internal standard, we can obtain lattice parameter of $a=3.267$ Å for ZnMgO and $a=3.254$ Å for ZnO. The chemical composition of the ZnMgO layer has been determined to be $Zn_{0.8}Mg_{0.2}O$ by TEM/EDS using a thin-foil specimen. The ω scan (rocking curve) result of different samples is shown in Table 1. The full width at half maximum (FWHM) values are smaller as the X-ray beam is perpendicular to the *c*-axis than it is in the parallel

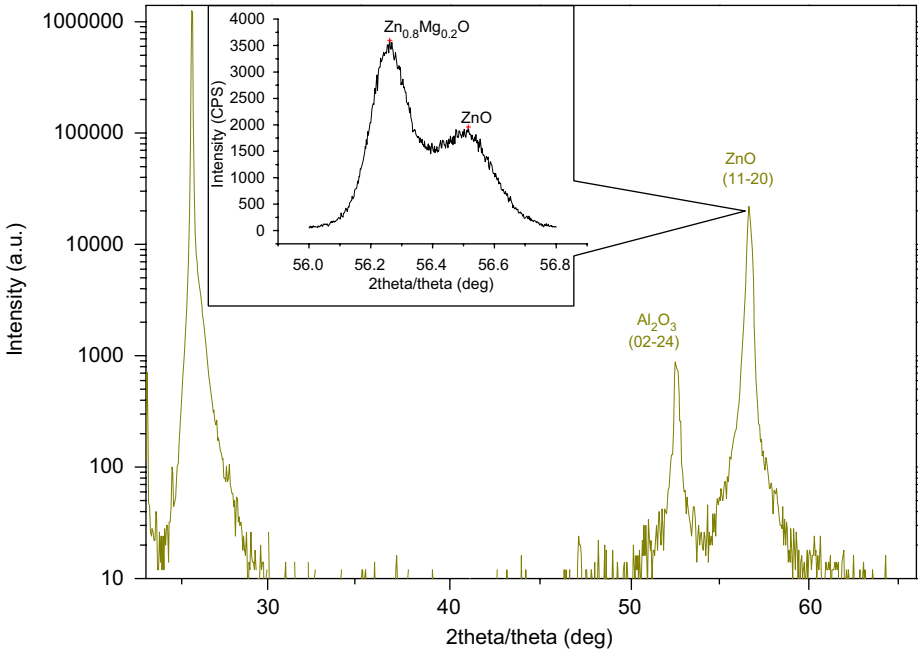

Fig. 1. X-ray diffraction pattern of ZnMgO/ZnO sample showing the ZnO *a*-plane peak around 56.5° in addition to the sapphire peaks in $2\theta/\theta$ scan.

azimuth. The difference can be as large as 400 arcs for the ZnMgO/ZnO and ZnMgO/ZnO five-period samples. Growth of *a*-plane GaN on *r*-plane sapphire also shows similar results as reported by Wang et al. [10]. It can be seen from the AFM morphology (Fig. 2) that only the ZnO sample shows plate-like grains, which also has the smallest value of FWHM and the smallest FWHM difference between the two X-ray azimuths. The rest samples show stripe morphology in which the direction of the stripes is parallel to the *c*-axis as shown in Fig. 2. This is due to anisotropic growth of zinc oxide, which has very strong tendency for growing along the *c*-axis. Except the ZnO sample, the deposited films exhibit a very smooth surface. However, as ZnO is thick enough, coalescence of the stripes in the thin films occurs, resulting in large islands with aspect ratio of about 2.5 and reduction of the FWHM value of the rocking curve.

Table 1
The ω-scan results of different samples

	XRD ω-scan FWHM (arcsec)		AFM roughness (nm)
	$\|c$-axis[a]	$\perp c$-axis	
ZnO	1229	998	2.75
ZnMgO/ZnO/Al_2O_3	2695	2270	0.89
ZnMgO/ZnO/Al_2O_3, 5 period	2056	1627	0.90
ZnMgO/ZnO/Al_2O_3, 10 period	2135	1803	0.99

[a]XRD beam was line focus and parallel to the *c*-axis of the films.

The epitaxial relationships were determined by *in situ* RHEED patterns, too. As shown in Fig. 3, RHEED patterns of various samples taken after deposition and cooling down the substrates to a high temperature can be compared with those at room temperature after cooling. Continuously sharp and streaky lines in the left column (at high temperature) can be clearly seen, indicating that the films at high temperature after deposition process are high-quality epitaxial ZnO with smooth surfaces for all samples. However, it degrades into 3D island morphology after being cooled down to room temperature, as can be seen that the lines in the right column become discontinuous. It is well known that ZnO and sapphire have anisotropic thermal expansion coefficients along *c*-axis ($8.5\times10^{-6}\,K^{-1}$ for sapphire and $3.02\times10^{-6}\,K^{-1}$ for ZnO at 300 K) and *a*-axis ($7.5\times10^{-6}\,K^{-1}$ for sapphire and $6.51\times10^{-6}\,K^{-1}$ for ZnO at 300 K). Also, there exists a large difference of thermal expansion coefficients between ZnO and sapphire. Therefore, it is not surprising that the significant change of characteristics of reflections in the RHEED patterns are observed after cooling. However, the ZnO sample which is about 500 nm thick shows high-quality characteristics even at room temperature, as shown in Fig. 3(d) for different incident directions of electron beam, consistent with the rocking curve data. It can be seen in the RHEED pattern that streaky lines remain for electron beam along [0 0 0 1], suggesting the surface is smooth in this direction, which is

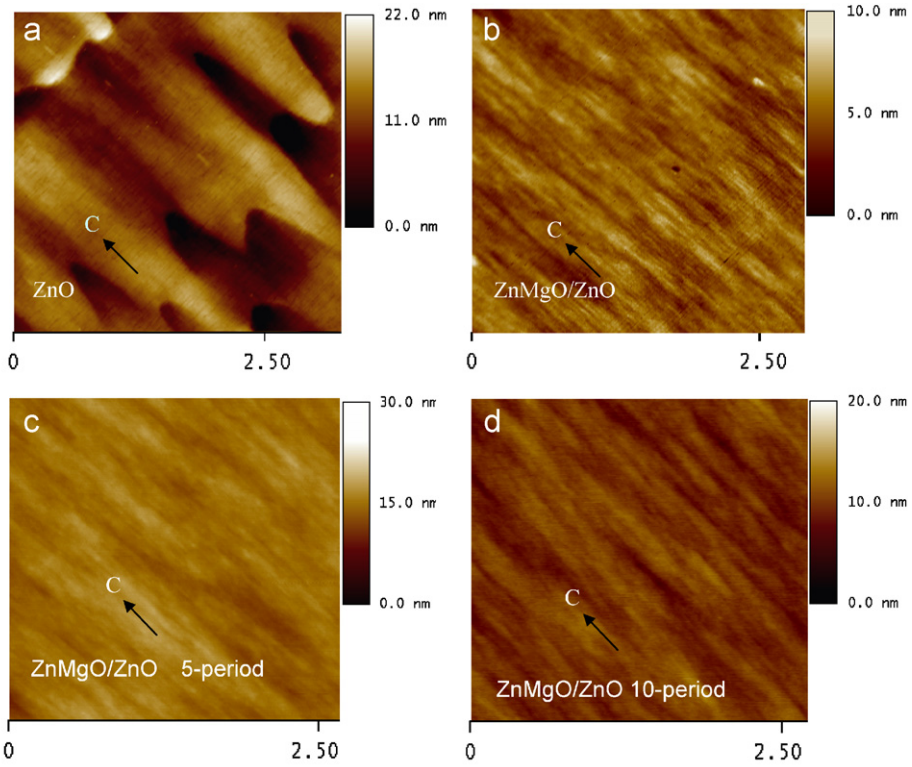

Fig. 2. AFM images showing (a) ZnO layer in plate-like morphology; and (b) ZnMgO/ZnO bilayer, ZnMgO/ZnO multi-layers of 5 periods (c), and 10 periods (d) in stripe-like morphology.

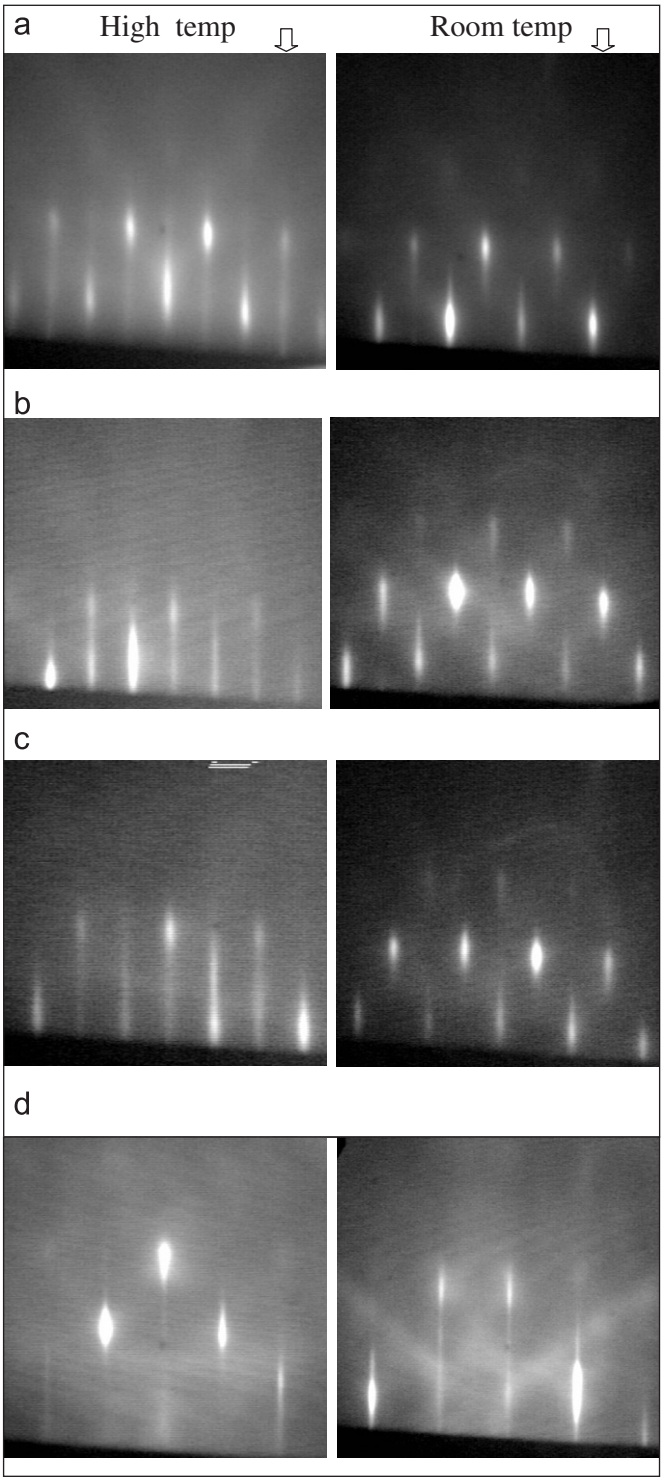

Fig. 3. RHEED patterns taken at room temperature (right column) and at high temperature for each sample (left column) (a) $T = 750\,^{\circ}C$ for the ZnMgO/ZnO 10-period sample, (b) $T = 638\,^{\circ}C$ for the ZnMgO/ZnO five-period sample, (c) $T = 630\,^{\circ}C$ for the ZnMgO/ZnO sample, and (d) RHEED patterns of ZnO sample at room temperature for incident electron direction perpendicular to (right) and along (left) *c*-axis.

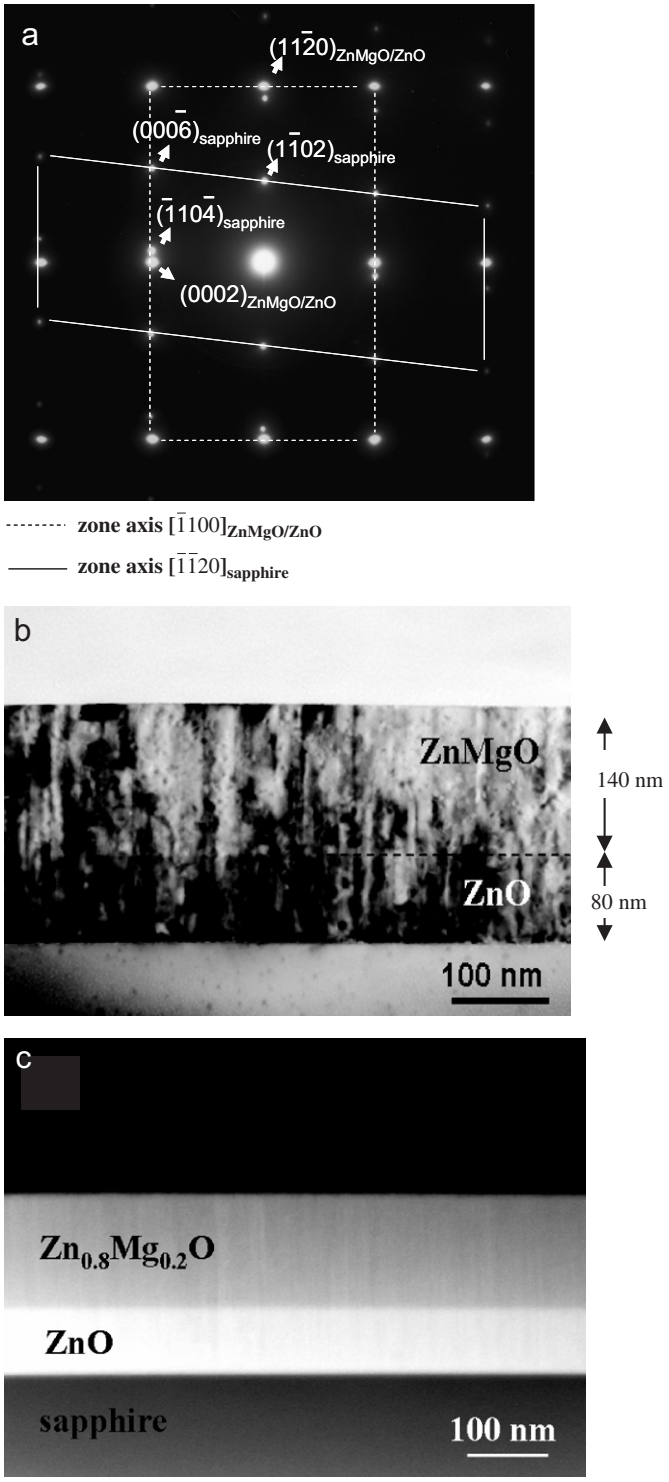

Fig. 4. (a) Selected area diffraction (SAD) pattern obtained from the interface between the ZnO layer and sapphire substrate, (b) BF cross-sectional TEM, and (c) STEM Z-contrast image of the ZnMgO/ZnO sample.

evident in AFM. The fact that the thick film in Fig. 3(d) degrades less than other films suggests that higher quality can be obtained at a larger thickness. As a result, the FWHM value in the rocking curve of the ZnO sample is smallest in all the samples. However, the AFM image shows large long islands rather than a continuous film.

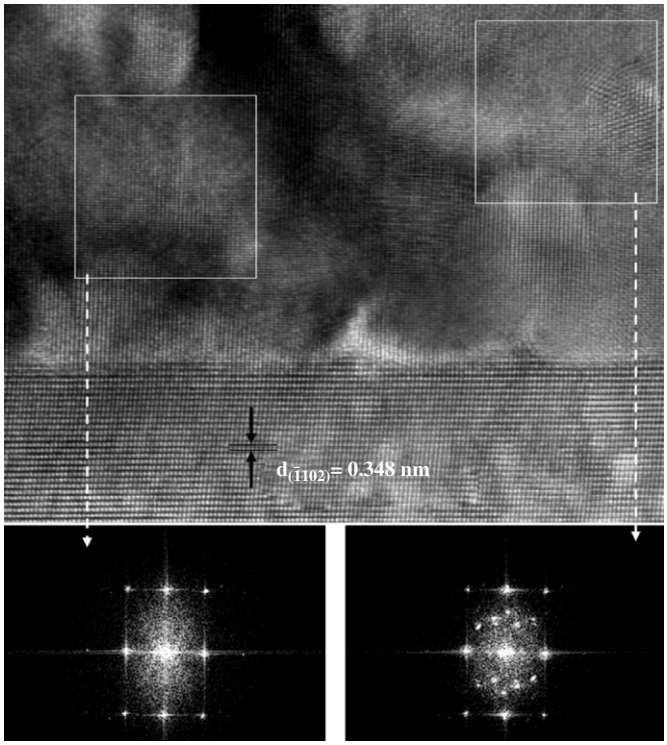

Fig. 5. HRTEM of the ZnMgO/ZnO bilayer sample with the corresponding fast-Fourier-transform (FFT) patterns from the framed regions.

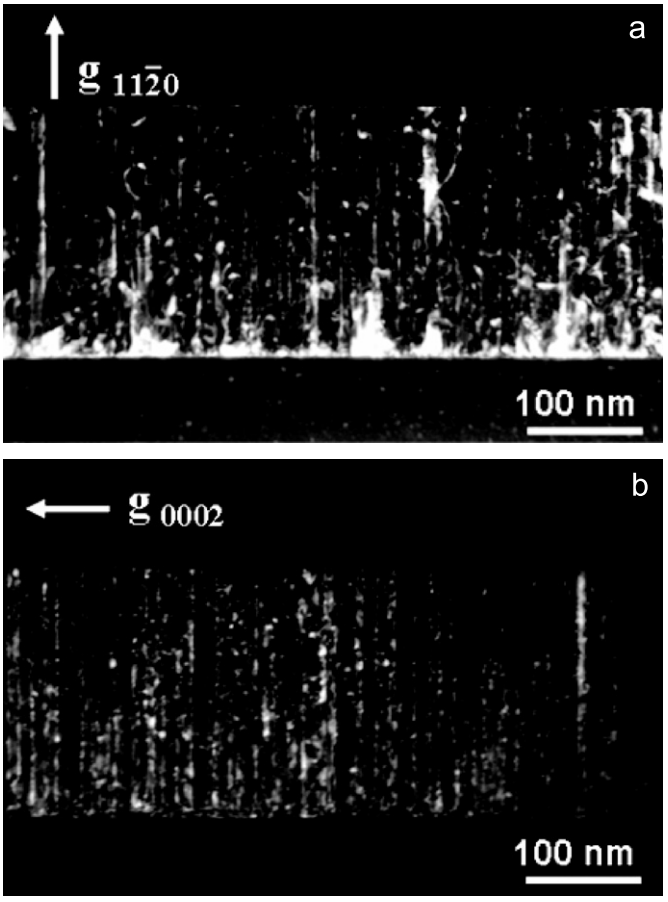

Fig. 6. g–$3g$ weak beam dark-field images taken near zone axis $[\bar{1}\,1\,0\,0]_{ZnO}$ with (a) $g = 11\bar{2}0$ and (b) $g = 0002$.

The selected area diffraction (SAD) pattern shown in Fig. 4(a) is obtained from the interface between the ZnO layer and sapphire substrate. The orientation relationship of ZnO with sapphire is determined to be $(1\,1\,\bar{2}\,0)_{ZnO}\|(0\,1\,\bar{1}\,2)_{sapphire}$. Observations from the bright-field (BF) TEM image and scanning TEM Z-contrast image in Fig. 4(b) and (c), the ZnMgO/ZnO and ZnO/sapphire interfaces are sharp, and the measured average thickness of ZnMgO and ZnO layers is ~140 and ~80 nm, respectively, suggesting that growth rate for ZnMgO and ZnO is approximately 2.4 nm/min at 650 °C and 3.6 nm/min at 800 °C, respectively. For the five-period ZnMgO/ZnO QW structure deposited at 650 °C, the growth rate is 3.5 nm/min for ZnO layer and 2.3 nm/min for ZnMgO layer as measured from STEM Z-contrast images (not shown). The fact that the growth rate of ZnMgO is lower than that of ZnO implies that ablation rate at the laser power is smaller for the ZnMgO target than the ZnO one.

According to diffraction contrast in ZnO and ZnMgO, it is also found that the grain growth of ZnMgO is continuous across the ZnMgO/ZnO interface. In Fig. 4(c), the uniform Z-contrast in the ZnMgO bilayer indicates that the Mg element is evenly distributed in the layer without any apparent MgO phase. Fig. 5 is a cross-sectional high-resolution TEM image of the interface between ZnO and sapphire taken from the electron beam direction along the *m*-axis of ZnO. The interface is observed to be atomically sharp for most of the regions. At a few places we can see extrusions on the sapphire surface where several ZnO grains with misorientations are observed as shown in fast-Fourier-transform (FFT) patterns. Therefore, the large FWHM values in X-ray rocking curves may be reasoned as a result of the uneven sapphire surface. Fig. 6 is g–$3g$ weak-beam dark-field images taken near zone axis $[\bar{1}\,1\,0\,0]_{ZnO}$ with (a) $g = 11\bar{2}0$ and (b) $g = 0002$, respectively. The measured dislocation density is approximately $2 \times 10^{11}\,cm^{-2}$.

4. Conclusion

ZnMgO/ZnO thin films in *a*-plane orientation were grown by PLD on *r*-plane sapphire with epitaxial relationship of $(1\,1\,\bar{2}\,0)_{ZnO}\|(0\,1\,\bar{1}\,2)_{sapphire}$ and $[0\,0\,0\,1]_{ZnO}\|[0\,\bar{1}\,1\,1]_{sapphire}$ as shown by XRD, RHEED, and TEM. The X-ray rocking curves, RHEED patterns, and AFM demonstrate anisotropic growth of ZnO and ZnMgO in the initial stage of deposition with very smooth surfaces at high temperature, which results in stripe morphology. After cooling down to room temperature, the large mismatch in thermal expansion degrades the surface smoothness. With the increase of film thickness, the morphology appears as 3D long islands due to the coalescence of the striped ZnO grains. TEM also shows that good epitaxy of ZnO occurs on the smooth surface of sapphire substrate with the sharp interface,

whereas extrusions on the sapphire surface result in disoriented ZnO grains.

Acknowledgments

This work was supported in part by National Science Council, Taiwan, ROC, under contracts NSC 95-2221-E-009-128 and NSC 95-2221-E-216-038.

References

[1] C. Morhain, T. Bretagnon, P. Lefebvre, X. Tang, P. Valvin, T. Guillet, B. Gil, T. Taliercio, M. Teisseire-Doninelli, B. Vinter, C. Deparis, Phys. Rev. B 72 (2005) 241.
[2] H.M. Ng, Appl. Phys. Lett. 80 (2002) 4369.
[3] C.H. Chia, T. Makino, K. Tamura, Y. Sega, M. Kawasaki, A. Ohtomo, H. Koinuma, Appl. Phys. Lett. 82 (2003) 1848.
[4] T. Moriyama, S. Fujita, Phys. Status Solidi (c) 3 (2006) 726.
[5] M. Tesseire-doninelli, G. Neu, Appl. Phys. A 88 (2007) 65.
[6] S. Muthukumar, J. Zhong, Y. Chen, Y. Lu, T. Siegrist, Appl. Phys. Lett. 82 (2003) 742.
[7] T. Moriyama, S. Fujita, Jpn. J. Appl. Phys. 44 (2005) 7919.
[8] S. Heitsch, G. Benndorf, G. Zimmermann, C. Schulz, D. Spemann, H. Hochmuth, H. Schmidt, T. Nobis, M. Lorenz, M. Grundmann, Appl. Phys. A 88 (2007) 99.
[9] V.A. Fonoberov, K.A. Alim, A.A. Balandin, F. Xiu, J. Liu, Phys. Rev. B 73 (2006) 165317.
[10] H. Wang, C. Chen, Z. Gong, J. Zhang, M. Gaevski, M. Su, J. Yang, M.A. Khan, Appl. Phys. Lett. 84 (2004) 499.